Electrical Activity of Boron and Phosphorus in Hydrogenated Amorphous Silicon

A. Pandey,[1] B. Cai,[2] N. Podraza,[3] and D. A. Drabold[4]

[1]*Department of Physics and Astronomy, Condensed Matter and Surface Science Program, Ohio University, Athens, Ohio 45701, USA*

[2]*Department of Radiation Oncology, Washington University School of Medicine, St. Louis, Missouri 63108, USA*

[3]*Department of Physics and Astronomy, University of Toledo, Toledo, Ohio 43606, USA*

[4]*Department of Physics and Astronomy, Ohio University, Athens, Ohio 45701, USA*

(Received 18 June 2014; revised manuscript received 9 September 2014; published 7 November 2014)

Using realistic models of hydrogenated amorphous silicon and density functional methods, we explore doping and transport with the most popular impurities: boron and phosphorous. We discuss conventional analogies of doping based upon shallow acceptors and donors in a crystalline matrix and highlight the limitations of such an approach. We show that B enters the network always with considerable strain, whereas P is much more "substitutional" in a tetrahedral site. We show that H is attracted to strained centers, especially for B, which increases the likelihood of H passivation effects on B impurities. We elucidate doping and nondoping static configurations in doped *a*-Si:H, and the role of H passivation as a partial explanation for the well-known low doping efficiency the material exhibits. We show that thermal fluctuations (that induce both network motion and H hopping) can also significantly impact conduction. We draw comparisons to experimental work.

DOI: 10.1103/PhysRevApplied.2.054005

I. INTRODUCTION

One can scarcely overestimate the importance of doping semiconducting materials. It is, of course, the basis of all electronic or optoelectronic applications (such as microbolometers for IR imaging [1], thin-film transistors for display control [2], and photovoltaic applications [2]). The experimental discovery that amorphous-silicon hydride (*a*-Si:H) could be doped with boron (*p* type) and phosphorous (*n* type) was due to Spear and LeComber in 1975 [3] and opened the door to the applications listed above.

To understand the work of Spear and Lecomber, researchers naturally began by adopting a shallow donor-acceptor picture for the doping based on experience with crystalline Si. It is worth noting, however, that there are problems with this picture. First, it is based on the assumption of translational invariance and, therefore, the assumption that all the (Bloch) states are extended. Only a decade before Spear and Lecomber, the community was greatly puzzled by the fact that *a*-Si even possessed a gap. This very basic fact was not easy to grasp at the time without long-range order, a point that Ziman emphasizes [4]. To understand the structure of the density of states near the Fermi level, it was shown that local order was all that was needed to ensure a gap, but it also highlighted the fact that reasoning based upon the conventional approach of applying the experience of crystalline Si could be misleading.

To delineate the key differences in doping between *a*-Si and diamond Si, we note the following: (1) The topological and chemical disorder of the *a*-Si:H structure creates a myriad of possible configurations, with highly variable electronic signatures. Mott immediately recognized this and noted that if B (for example) was not fourfold, it could not be expected to dope the network. In fact, there are other possibilities besides nonsubstitutional coordination: there might be angular strains, bond length strains, H nearby in one of the various sites, etc. (2) There is much more thermally induced variation in the coordinates of the atoms in the *a*-Si matrix than in diamond, and this has many consequences. The picture of small oscillations and phonons needs to be carefully considered for topologically disordered systems [5]. One signature of the difference between crystalline and disordered systems is the anomalous low-energy excitations of the amorphous network (tunneling modes, Boson peak, etc.) and the ambiguous nature of the structural ground state for a topologically disordered system [6]. (3) It turns out that the electronic response from these fluctuations is very strong, most particularly, around the optical gap where electron states are localized [7]. From the Kubo formula, it is evident that these are also the states that play a critical role in transport. (4) H also plays an essential role. No material of electronic utility is without H. H is highly mobile at temperatures above room temperature [8], and as it hops, its electrical activity can change, and, thus, it can also impact doping.

A great deal of experimental work has been carried out on doped *a*-Si:H, including NMR experiments [9] that gave valuable clues about the doping process. Furthermore, the ideas of the preceding were developed much further by considering thermal equilibrium of the various state (the "doping model" [2]). This was done with kinetic equations

and actually has much in common with the basic spirit of this paper, which starts with atomistic models and explicitly reveals important structures and dynamical processes that underlie such a picture.

To summarize our results, we report a wide range of accessible configurations using accurate molecular dynamics calculations. We detail the strain effects that arise from placing P and B in realistic models of *a*-Si:H. We show that B is intrinsically highly strained, and P is far more "substitutional." We prove with current techniques that the old conjecture of Boyce and Ready [9] that H passivation is, indeed, a key reason for low doping efficiency, also discussed earlier by Fedders and Drabold [10] and by Cai and Drabold [11]. We show that the results are reproducible; similar results accrue for impurities substituted into similar sites. By starting with the Kubo-Greenwood formula, we show that the dynamics of the lattice and the H play an essential role, at least at higher temperatures (say, 300 K and above). We show that under certain circumstances, conductivity is strongly enhanced by transient doping conformations.

From the standpoint of photovoltaic applications, Schiff and co-workers [12] argue that the broad valence-band tail in *a*-Si:H solar cells limits the efficiency of the devices. We show, perhaps unsurprisingly, that a maximally structurally homogeneous network [13] leads to a narrow valence tail [14,15]. Here, we note that because of the large strain associated with B (bond lengths even in a tetrahedral environment of order 0.3 A shorter than the Si mean bond length), it is likely that the broad valence tail [2] is inherent to the B-doped system, and it makes one wonder if an alternative approach to acceptor doping might lead to better results.

Like any simulation being compared to real materials, our work has limitations. First, we implement all the simulations in the local-density approximation of density functional theory. This is a reliable approximation for important relaxation effects, but it is well known to badly underestimate the gap. The placement of defect and impurity states is, therefore, only qualitative. For a more quantitative approach, the current method of choice is probably the HSE functional [16], which also involves significantly larger computational expense. In addition, no simulation on small supercell models can capture all possible configurations. For low concentrations of impurities, however, it is possible to report representative structures, and we attempt to consider some configurations that involve clustering of the dopants. The stability of structures and the dynamical response of H (moving to reduce strain) is also apparent from thermal molecular dynamics (MD) simulations reported in Sec. IV. Our calculations are illustrative but are not exhaustive. It is also apparent that the process of doping *a*-Si:H is not "simple." There are many different conformations possible for dopants and H, and the electrical activity and formation energy of these vary. Our work may be understood to be a partial catalog most salient for low concentrations of impurities. Higher concentrations can be handled by extended simulations (based upon the Monte Carlo method or MD with *ab initio* total energies and forces) that sample a fuller configuration space. The equilibrium distribution of configurations of defects depends on the formation energy of the defects (which we do not compute) and the detailed growth processes in the particular film. We do not simulate the growth; so in our calculations, we adopt a preexisting realistic albeit small model and study defects (including all relaxation effects) in the context of that model. Since even the basic electronic attributes of these structures is unknown, our simulations are a valuable addition to the literature of *a*-Si:H.

This paper offers a partial treatment of the role of dynamics, primarily serving notice that the motion of the lattice as well as H hopping is important to understanding doping. We show that H is attracted to B sites, in response to strained bonds that occur there. Clearly, this increases the probability for H occupying the neighborhood of B atoms, though we have not quantified this effect. Since we show that H passivates doping, this provides a qualitative explanation for the low doping efficiency of B in Si.

The rest of this paper is organized as follows. In Sec. II, we describe computational methodology and the structural models employed. In Sec. III, we consider a realistic static model with impurities and H placed in many positions, with attention paid to relaxation effects, and we catalog the electronic consequences of these placements. In Sec. IV, we allow everything to move—host and H—and discuss the conductivity from the standpoint of the Kubo formula and elucidate the importance of H hopping in creating transient doping conformations. Conclusions are given in Sec. V.

II. METHODOLOGY AND MODELS

In our simulations, we employ the Vienna *ab initio* Simulation Package (VASP), a quantum-mechanical molecular dynamics package using a plane-wave basis set and the local-density approximation [17]. The electron-ion interactions are described using the projector augmented-wave method [18]. A 64-atom amorphous-silicon cubic cell of side 10.854 Å generated by Barkema and Mousseau [19] then annealed and relaxed by us, is used as a starting model for the calculations. Boron (B) and phosphorous (P) atoms are introduced on various tetrahedral Si sites in the network and then relaxed at constant volume using the conjugate gradient method. Models are fabricated with concentrations 1.6%, 3.1%, 7.8%, and 12.5% of B and P for a static study of doping. Hydrogen passivation in B- and P-doped systems is studied by introducing H atoms at various sites in the 1.6% B- and P-doped *a*-Si models. One calculation is carried out on a 216-atom model made by the same group [19].

Dynamical simulation is carried out on 3.2% B- and P-doped *a*-Si models, and H atoms are introduced in bond centers (BCs) at varying distances from the impurities. The data presented here are for 80-ps time evolution with a time step of 2 fs. For selected cases, we double this time to verify our results. These times are adequate to reveal important thermal processes, though not to offer a full sampling of the phase space.

III. IMPURITIES ON A STATIC LATTICE

The purpose of this section is to determine doping and nondoping configurations in B- and P-doped *a*-Si and also to understand the effect of hydrogen in doping. The electronic density of states (EDOS) is calculated for models doped with varying concentrations of B, P, and hydrogen. Initially, the EDOS of 64-atom *a*-Si (Wooten-Winer-Weaire model) [20] and 8.5% H-doped *a*-Si, 70-atom *a*-Si:H model is studied as shown in Fig. 1. For both models, there is a clear gap, and the Fermi level is in the gap, and we, therefore, interpret these models as representing a nondoped conformation.

Further analysis is carried out with different concentrations of B and P doped on the 64-atom *a*-Si. Doping is studied initially by substituting impurities on highly tetrahedral Si sites. For the 1.6% doped system, we investigate the H passivation.

A. Boron- and phosphorous-doped *a*-Si

When impurities such as boron and phosphorous are introduced into a network of *a*-Si, the Fermi level may shift toward a band edge. We study seven different models of B-doped *a*-Si, as shown in Fig. 2. We calculate the EDOS for all the models with the Fermi level shifted to zero in each case. The models are described in Table I.

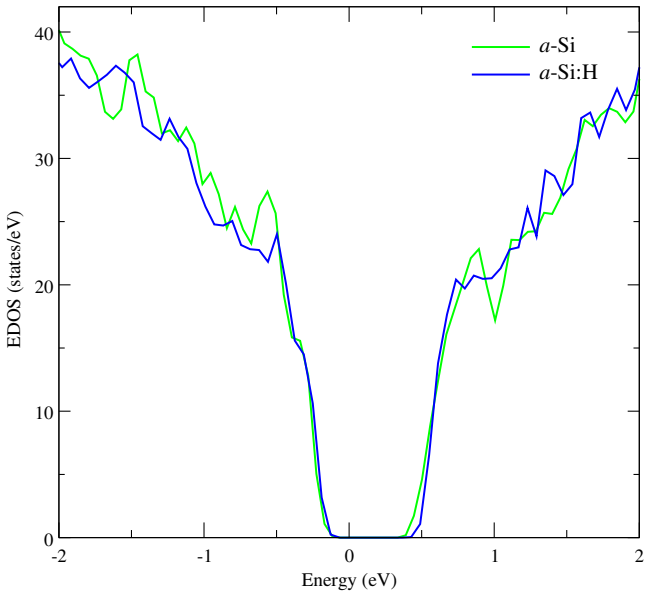

FIG. 1. Electronic density of states (EDOS) with Fermi level at 0 eV. Green represents the EDOS for 64-atom *a*-Si and blue is the EDOS for 70-atom *a*-Si:H.

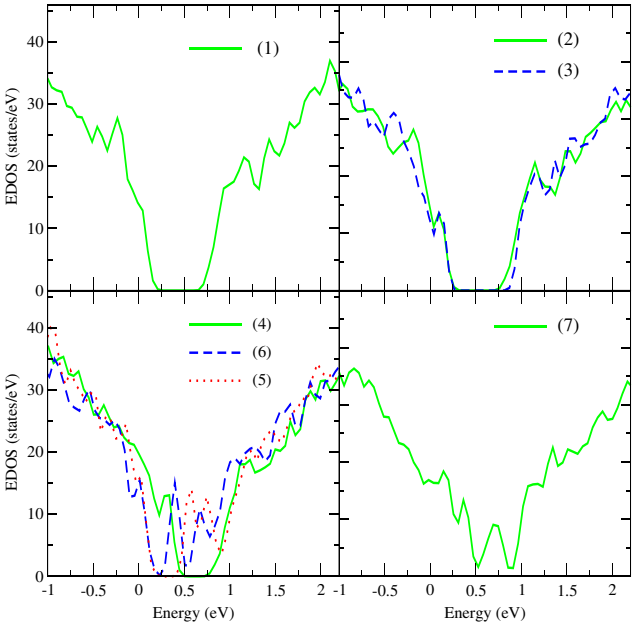

FIG. 2. Boron-doped *a*-Si with various impurity concentrations. Models (1), (2), (4), and (7) are 1.6%, 3.1%, 7.8%, and 12.5% B-doped *a*-Si, respectively, with each B having configuration B(4Si) (four Si neighbors to B). In models (3) and (5), B dimers are formed with configuration B(3Si,1B). Model (6) consists of a B4 cluster with configuration B(1Si,3B). Details of these models are provided in Table I. The Fermi energy is at 0 eV for each curve in the figure.

In Fig. 2, there are four panels that report the EDOS for seven different models, as stated in the index of the panels. In models (1), (2), (4), and (7) of Fig. 2 all B atoms are "separate" in the sense that each boron is fourfold coordinated with Si atoms which are denoted by B(4Si) and there is no B—B bond. All of these models represent a doped configuration with the gap cluttered with states for model (7). As the B concentration increases, more valence tail states are formed, and the states move into the gap, as can be seen in model (7).

In each case, there are three shorter bonds and one longer bond with the bonds highly strained. The average over the configurations for the four B—Si bonds are, respectively, 2.02, 2.04, 2.07, and 2.16 Å. These bond lengths are highly strained compared to the mean bond length of Si—Si, which is 2.34 Å [10], and in the spirit of our work on Urbach tails, can be thought of as inducing a strain field associated with the valence edge [14]. These strains create long bonds in the next nearest neighbor of B, with second-nearest-neighbor bond lengths near 2.5 Å. This effect is also observed in a large model of 215 Si atoms doped with a B atom at a perfectly tetrahedral Si site. It is observed that the average bond length for the first-nearest-neighbor atom shell of B is 2.05 Å and the second-nearest-neighbor shell is

TABLE I. Static boron configurations.

Fig. 2	Models n(B), n(Si)	B clustering	Config.	Electrical activity
1.	1B,63Si	Separate	B(4Si)	p doped
2.	2B,62Si	Separate	B(4Si)	p doped
3.	2B,62Si	B dimer	B(3Si,1B)	p doped
4.	5B,59Si	Separate	B(4Si)	p doped
5.	5B,59Si	B2 cluster	B(3Si,1B)	p doped with defects
6.	5B,59Si	B4 cluster	B(1Si,3B)	p doped with defects
7.	8B,56Si	Separate	B(4Si)	Many defect states

2.45 Å. From the third-nearest-neighbor shell, there is no significant departure from the mean bond length of the a-Si network.

In model (3), the B is clustered, so that each B atom is bonded to another B atom and three other Si atoms and denoted by B(3Si,1B) forming a B dimer. These conformations induce doping so long as B atoms are fourfold. However, when B clusters are formed, additional defect states appear near the conduction-band tail, and they clutter the gap as can be seen for model (5) and model (6). The configuration for model (5) is comprised of B2 clusters (B dimer), in which B atoms are bonded with another B atom and three Si atoms and are denoted by B(3Si,1B). There are two such dimers in model (5). In model (6), B4 clusters are formed, which is one B bonding with three B atoms and one Si atom and is denoted by B(1Si,3B). These midgap states arise from defects which are mainly the under- and overcoordinated Si atoms. These configurations are shown in Table I.

As a summary of the static study of B-doped amorphous Si, the tetrahedral B dopes the a-Si network and shifts the Fermi level towards the valence-band tail as expected from elementary considerations. Increasing the concentration of B introduces defect states in the gap which are mainly due to Si dangling bonds (DBs) and floating bonds, probably arising from the strained (short bonds) between B and Si.

In the study of P-doped a-Si, we calculate the EDOS of eight different models in four panels, as shown in Fig. 3 with the Fermi energy shifted to zero. The EDOS of models (1), (2), (5), and (8) are for 1.6%, 3.1%, 7.8%, and 12.5% P-doped a-Si, respectively. In these models, P atoms are substituted in perfectly tetrahedral Si atom sites, deep donor states are formed, and the Fermi level shifts towards the conduction-band tail and the systems are n-type doped.

The average bond length of P atoms formed with Si atoms (in tetrahedral sites) are 2.32, 2.31, 2.28, and 2.24 Å, respectively. These are close to the average Si—Si bond length. There are eight different models presented in Fig. 3. In models (1), (2), (5), and (8), the P atoms are separate, which means each P atom is bonded to four Si atoms and there is no P—P bond. The configuration is denoted by P(4Si). In model (3), a P2 dimer is formed in which each P is bonded with another P atom and three Si atoms which is denoted by P(3Si,1P). In model (4), P is threefold, which means each P is bonded to three Si atoms and is denoted by P(3Si). Model (4) consists of a P4 cluster where each P forms a bond with three other P atoms and a Si atom. The P4 cluster is denoted by P(1Si,3P). Model (7) comprises a mixture of a P2 dimer and P3 cluster. The configuration for the P2 dimer is denoted by P(3Si,P) and for the P3 cluster, it is P(2Si,2P). Our configurations are summarized in Table II.

It can be seen that as the concentration of P increases, more defect states are formed near the conduction-band edge [see model (8)] that eventually closes the gap. As long as the P is tetrahedral, P dimers dope the system, as can be seen in model (3) and model (7) with defect tail states.

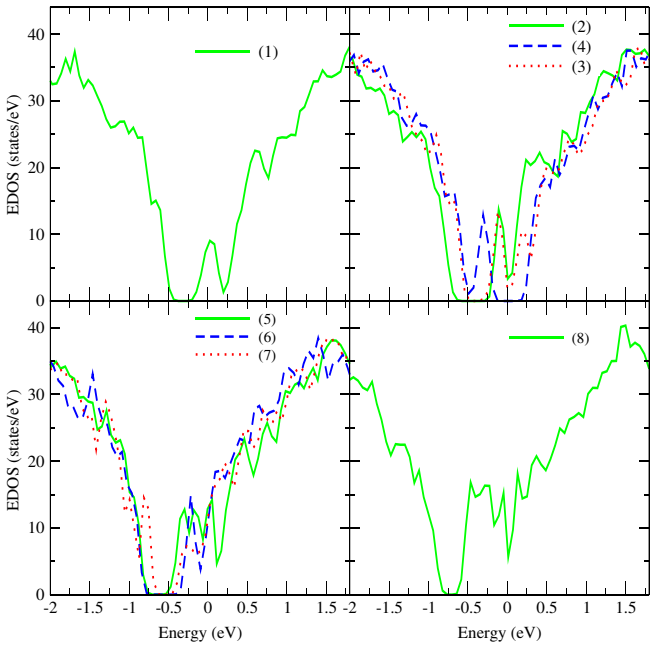

FIG. 3. Phosphorous-doped a-Si with different impurity concentrations. Models (1), (2), (5), and (8) are 1.6%, 3.1%, 7.8%, and 12.5% B-doped a-Si, respectively, with each P having configuration P(4Si). In models (3) and (7), the P dimers are formed with configuration P(3Si,1P), and model (6) consists of a P4 cluster denoted by P(1Si,3P). P is threefold in configuration (4) with configuration P(3Si). Details of these models are provided in Table II. The Fermi energy is at 0 eV for all the EDOS in the figure.

TABLE II. Static phosphorous configurations.

Fig. 3	Models n(P), n(Si)	P clustering	Config.	Electrical activity
1.	1P,63Si	Separate	P(4Si)	n doped
2.	2P,62Si	Separate	P(4Si)	n doped
3.	2P,62Si	P dimer	P(3Si,1P)	n doped
4.	2P,62Si	Threefold P	P(3Si)	Undoped with defects
5.	5P,59Si	Separate	P(4Si)	n doped
6.	5P,59Si	P4 cluster	P(1Si,3P)	n doped
7.	5P,59Si	P2 or P3 cluster	P(3Si,1P), P(2Si,2P)	n doped
8.	8P,56Si	Separate	P(4Si)	Gap filled with tail states

The configuration is undoped for threefold P shown in model (4). In model (6) and model (7), P clusters also dope the system if P is tetrahedral.

As a summary for the static study of P-doped amorphous Si, tetrahedral sites dope the system by shifting the Fermi level towards the conduction-band tail, while threefold P leads to a nondoping configuration. Increasing the concentration of P produces more defect states in the gap as the network rearranges to produce more threefold and fivefold Si atoms.

The most notable contrast between B and P doping is a large local strain around B and a more substitutional character for P. This strain seems to be relevant to the work of Schiff concerning broad valence tails [12].

B. H passivation in hydrogenated B- and P-doped *a*-Si

The efficiency of doping is highly influenced by the presence of hydrogen in a network. H passivates the dangling bonds present in the network and opens the optical gap, whereas bond center H near impurities poisons the doping and reduces the doping efficiency. To study these properties, H atoms are introduced in B- and P-doped *a*-Si, and their effect in doping is studied in terms of the shift in the Fermi energy level in EDOS.

To study the role of hydrogen in B- and P-doped *a*-Si, H atoms are introduced at various sites of the network, thereby forming initial metastable structures. These structures are then relaxed to find a stable configuration. The effect on doping is studied by calculating the EDOS to observe the shift in the Fermi level. We discuss first the H passivation in B-doped *a*-Si, and then we discuss the P-doped system.

In Fig. 4(a), H is initially attached to a B atom forming a metastable configuration B(4Si,1H) (B forming bonds with four Si atoms and one H atom). After relaxation, H breaks a B—Si bond and forms B(3Si,1H), a B bonded with three Si atoms and one H atom, structure with a Si DB. This configuration is nondoping, as the Fermi level shifts into the gap with a defect state due to the creation of a Si DB (Fig. 5). However, if another H passivates the Si DB, the Fermi level shows *p*-type activity. Thus, we can conclude that B(3Si,1H) with Si DB poisons doping, and B(3Si,1H) without a Si DB is an effective doping configuration, which is consistent with other work [10,11].

Next, we place a hydrogen atom at a Si—Si BC near B, and study its effect on doping. We find that H is stable in BCs, and in this configuration, it suppresses the doping. We study two different cases of H passivation: the first with H at a BC of a second nearest neighbor of B and the second at a third nearest neighbor of B atom (Fig. 6). In the top panel of Fig. 6(a), H is initially bonded to a Si neighbor of B, and after relaxation, H breaks the Si—Si bond and stays at the BC forming a B-Si-H-Si structure [top panel of Fig. 6(b)]. The EDOS of this structure shows that the Fermi level shifts into the gap, thereby suppressing the doping [Fig. 7 (left)]. A similar study is carried out for H initially bonded to the second-nearest-neighbor Si of a B atom, and after relaxation, it moves to the BC forming a B-Si-Si-H-Si structure, as shown in the lower panel of Figs. 6(a) and 6(b). The EDOS of this structure shows that the Fermi level is shifted towards the gap suppressing doping [Fig. 7 (right)]. These results indicate that the BC H, sufficiently close to the B atoms poisons the doping.

In all the above cases, B remains in a tetrahedral conformation after relaxation, and there is no Si DB left in the network and no defect states in the gap. In Ref. [21], it is suggested that at low B concentration holes can be trapped at strained Si—Si bond centers [22]. The charge due to these trapped holes may be compensated by a H atom trapped in the bond centers. In *a*-Si:H, B(4Si,1H) forms a stable configuration, but when an electron is

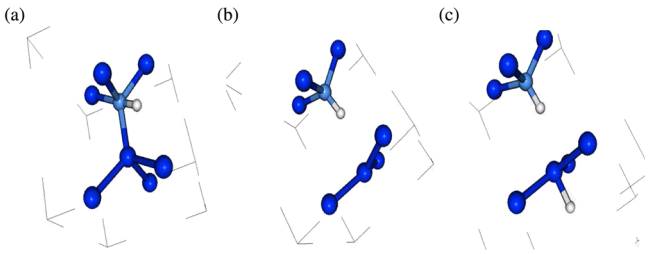

FIG. 4. H passivation in B-doped *a*-Si. (a) H bonds with B forming a metastable B(4Si,1H) structure. (b) Relaxation breaks a Si-B bond forming B(3Si,1H) and a Si DB. (c) Another H passivates the Si DB (dark blue, Si; light blue, B; white, H).

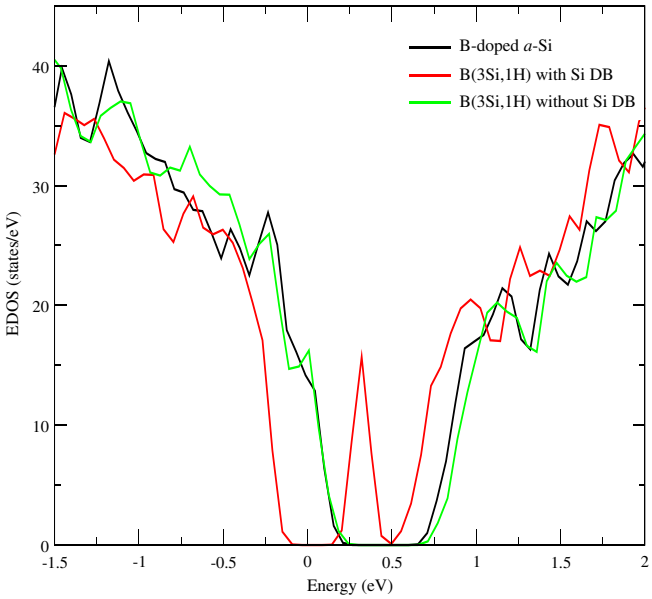

FIG. 5. Comparison of EDOS for different configurations in H passivation for B-doped *a*-Si. Green denotes the EDOS of B bonded with 3Si and 1H without a Si dangling bond, which is a doped configuration. Red is the EDOS of B bonded with 3Si and 1H with a Si dangling bond and is an undoped configuration with a defect state in the gap. The Fermi level is shifted to 0 eV in all the EDOS.

removed from the system, the Si—Si bond breaks and H occupies the BC position.

In P-doped *a*-Si, H passivation is studied in a similar way as the B-doped *a*-Si. H is initially bonded with a P atom forming a P(4Si,1H) metastable structure. After relaxation, the Si-P bond breaks, and H sticks to P forming a P(3Si,1H) structure with a Si DB. When another H is added to the

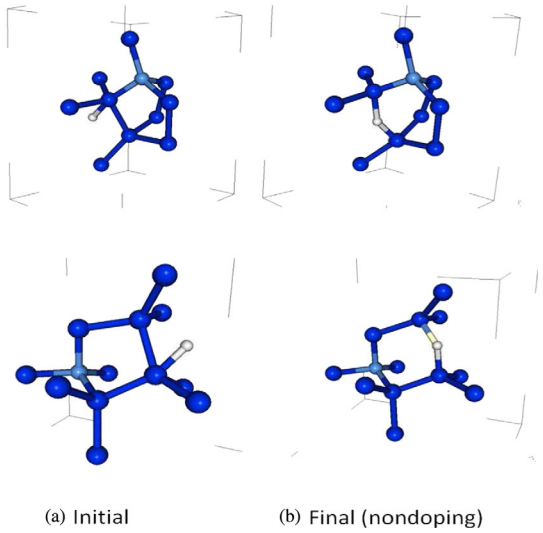

FIG. 6. (a) H attached to a first nearest neighbor of B (top panel) and second nearest neighbor of B (bottom panel). (b) Bond center H forming structures B-Si-H-Si (top panel) and B-Si-Si-H-Si (bottom panel).

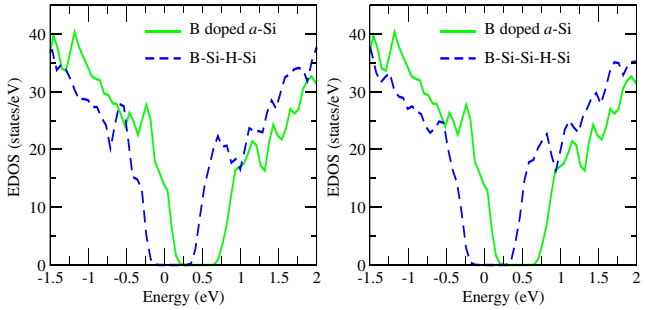

FIG. 7. (Blue left) EDOS for the B-Si-H-Si BC structure after relaxation which is undoped. (Blue right) EDOS for the B-Si-Si-H-Si BC structure after relaxation which is undoped. Green is the EDOS of B-doped *a*-Si and is a doped configuration. The Fermi level is shifted to 0 eV in all the EDOS.

system, the Si DB is passivated (Fig. 8). The EDOS of these structures are shown in Fig. 9. For the P(3Si,1H) structure, the Fermi level shifts in the gap with a defect state due to a Si DB, thereby poisoning the doping. When Si DB is passivated by another H, the configuration is doped. Thus, we conclude that P(3Si,1H) without Si DB is an effective doping configuration for H close to the P atom.

We study two cases for H passivation in P-doped *a*-Si. H is initially placed at the BC of P—Si, forming a P-H-Si structure and then relaxed. It is observed that the P—H bond breaks, leaving P threefold, and the H atom bonds with Si, as shown in the top panel of Fig. 10. In the EDOS of later configuration, the Fermi level shifts into the gap, making the system undoped [Fig. 11 (left)]. In another case shown in the bottom panel of Fig. 10, H is placed in the BC on the first- and second-nearest-neighbor Si atoms of P, at the Si—Si BC and forming a P-Si-H-Si structure, and then relaxed. The network reconstructs, and P becomes threefold and H sticks to a Si DB. The EDOS displays the suppression of doping without defects states [Fig. 11(right)].

In contrast to the H passivation in B-doped *a*-Si, H does not prefer the bond-center position in P-doped *a*-Si. Instead, it passivates Si DB. This result is consistent with NMR experiments which predict that in P-doped *a*-Si:H, about 40% of the H atoms are in the second nearest neighbor of P [9].

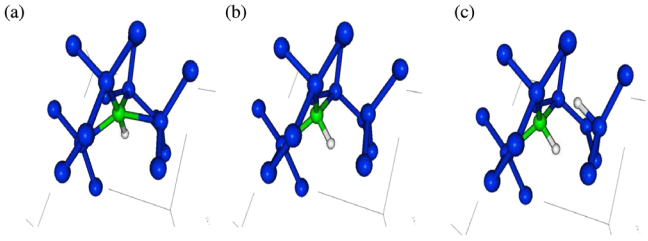

FIG. 8. H passivation in P-doped *a*-Si. (a) H bonds with P forming a metastable P(4Si,1H) structure. (b) Relaxation breaks a Si-P bond forming P(3Si,1H) and a Si DB. (c) Another H passivates the Si DB (dark blue, Si; green, P; white, H).

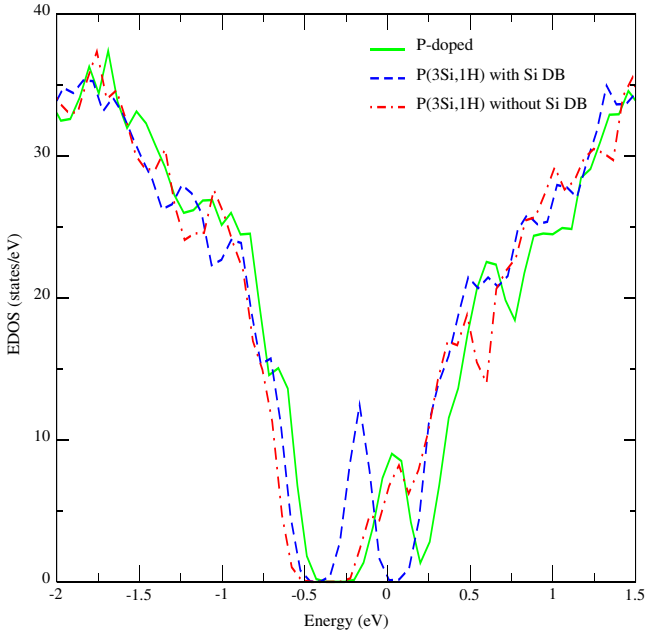

FIG. 9. Comparison of EDOS for different configurations in H passivation for P-doped *a*-Si. Blue is the EDOS of the final configuration in which P bonds with 3Si and 1H atoms with a Si dangling bond. Red is the EDOS of the final configuration in which P bonds with 3Si and 1H without a Si dangling bond. The Fermi energy is shifted to 0 eV in all the EDOS.

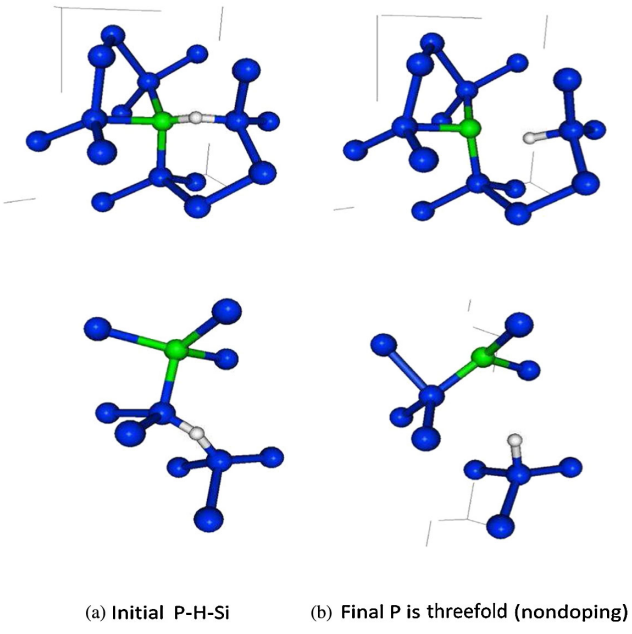

FIG. 10. H passivation in P-doped *a*-Si. (a) Top panel forming a P-H-Si structure and bottom panel forming a P-Si-H-Si structure. (b) After relaxation, P forms a threefold bond, and H passivates Si DB producing a nondoping configuration (blue, Si; green, P; white, H).

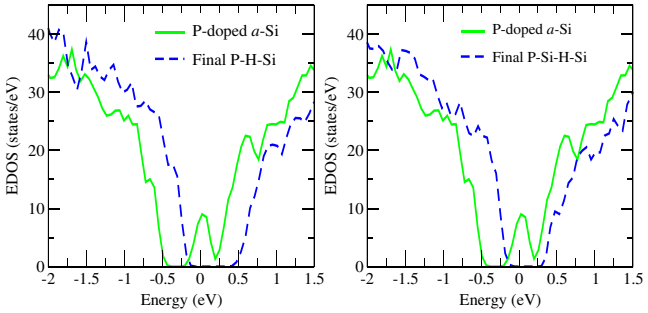

FIG. 11. EDOS for the two H passivation cases. (Left) Initial P-H-Si structure after relaxation forms P(3Si) and Si(3Si,1H). (Right) Initial P-Si-H-Si structure after relaxation forms P(3Si) and Si(3Si,1H). The Fermi level is shifted to 0 eV in all the EDOS.

Thus, tetrahedral B and P dope the system, but a high concentration of B and P impurities introduce midgap states. Clusters of impurities also create defect states in the gap, leading to compensation effects. The low doping efficiency is partly due to H passivation. An *a*-Si network doped with B and P has a higher number of under- and overcoordinated Si and H in such amorphous network and passivates the Si DB (threefold Si), thereby increasing the doping efficiency. We find that B(3Si,1H), P(3Si,1H), and Si(3Si,1H) are effective doping states. The hydrogen atom prefers to stay at a nearby bond center for B-doped *a*-Si, while in P-doped *a*-Si, it prefers to bond with a Si dangling bond leaving P threefold.

C. Experimental connections

The experimental results for the macroscopic properties most readily associated with doping, film resistivity, can be explained within the context of these theoretical models. Even though these theoretical results are applicable only for small subsets of atoms contained within a macroscopic film, the overall qualities of these subsets and bonding configurations may be simultaneously present in fabricated material with one dominant structural type.

a-Si:H-based materials fabricated by plasma-enhanced chemical vapor deposition (PECVD) have found the greatest utility in electronic applications and, therefore, are measured the most extensively in literature. Some of those results identify relationships between film resistivity and processing parameters. In PECVD, the ratios of hydrogen gas (H_2) and the respective *n*- or *p*-type doping gas to silicon-carrying gas, most commonly silane (SiH_4), are strongly linked to the electrical performance and are commonly varied. Typical doping gases include phosphine (PH3) to produce *n*-type material and diborane (B_2H_6), boron trifluoride (BF_3), boron trichloride (BCl_3), or trimethylboron [$B(CH_3)_3$] to produce *p*-type material.

To increase the amount of impurity atoms in the film, the doping-gas-to-silicon-carrying-gas ratio is increased, although this procedure does not monotonically alter film resistivity [23,24]. For both *p*- and *n*-type films, resistivity

decreases with the addition of low to moderate amounts of doping gas. A minimum is reached, and the addition of more doping gas corresponds to a slow increase in resistivity. Although these trends commonly appear, precise relationships between resistivity and the doping-gas-to-silicon-carrying-gas ratio depend on the type of doping gas as well as other PECVD parameters such as electrode spacing, plasma excitation frequency, plasma power density, substrate temperature, processing pressure, and the presence and amounts of additional gases such as H_2. The initial resistivity decrease in both B- and P-doped *a*-Si:H could be due to small amounts of these atoms not significantly straining the network and retaining fourfold coordination. After the minimum in resistivity is reached, additional dopant atoms adopt either five- or threefold coordination for B and P, respectively. These excess impurities may either (1) simply not locally shift the Fermi level away from the gap as described in the theoretical modeling or (2) sufficiently distort the network so that fewer doped atoms are fourfold coordinated. As the resistivity does not remain at the minimum with additional impurities, the second explanation likely occurs in conjunction with the first. These trends have been observed for both *n*- and *p*-type *a*-Si:H in Refs. [23,24].

Variations in resistivity with H_2 dilution have also been observed for both doping types [21,25,26]. Generally, material made at low-H_2 dilution remains amorphous throughout growth; however, sufficient dilution can result in the nucleation and subsequent growth of crystallites from the amorphous phase under appropriate conditions [27]. For amorphous films, initial increases in the H_2 dilution correspond with an increase in resistivity. Resistivity reaches a maximum and then decreases with further dilution up to the onset of crystallinity [26]. Crystallite inclusions then result in additional decreases in resistivity, as expected due to the higher doping efficiency of impurities within a crystal lattice [21,23,26]. The initial increase in resistivity within the amorphous phase may be due to small amounts of hydrogen being incorporated into the network; however, not enough is present to generate B(3,1) or P(3,1) configurations and passivate nearby dangling bond defects. The fourfold impurity acts as a dopant, but the electron or hole so produced can be taken up in a nonconducting dangling bond site. After sufficient hydrogen is introduced into the process, more B and P atoms may occupy (3,1) configurations with nearby dangling bonds passivated.

Sometimes nonmonotonic behavior in resistivity with H_2 dilution exhibits more than one increase and decrease. PECVD and the *a*-Si:H network is simply much more complex than these theoretical models. The silicon-hydrogen-bonding configuration (Si-H_n, $n = 1, 2, 3$) has also been linked to material electronic quality [28–30]. Larger-scale variations such as the formation of divacancies, nanoscale voids, and variations in overall film density have been detected in the infrared to visible range optical properties [21,28–31]. Whenever hydrogen and impurity atoms are introduced jointly, there can be interplay between order induced among the silicon atoms in the network and the functionality of the dopant atoms. Furthermore, the characteristics of the plasma originating from the choice of gases and other conditions and underlying the substrate material control the degree of order within the network [27]. Atomic hydrogen during PECVD can etch or rearrange weakly bound material at the film surface during growth [32]. This rearrangement can result in a more ordered network with fewer strained sites required to stabilize the material. Additional hydrogen introduced along with impurity atoms can passivate dangling bonds and increase the total doping efficiency of impurity atoms within the film.

Further studies focusing on the impact of deposition parameters on carrier mobility, carrier concentration, impurity atom concentration, and B, P, and Si-H_n infrared active chemical bonding modes [28–31,33,34] on common samples could be used to identify more precise relationships between film composition, structure within the network, and electrical response.

IV. DYNAMICAL LATTICE

We perform thermal MD simulations of hydrogenated *a*-Si doped with B and P at different temperatures (300, 400, 600, 800, and 1000 K). Note that for temperatures above 600 K, laboratory samples lose H, with commensurate changes in structure and conduction. We consider temperatures above this to observe rare events in the network dynamics, H hopping, and electronic structure. We track the trajectories and bonding of all the atoms. We also study the doping in these systems, which, in certain cases, are evolving or fluctuating with time.

The dynamical variable chosen to probe this is the HOMO LUMO gap, ξ, and the reason behind it is based on defining the doping in terms of the conductivity which depends on this dynamical variable (since the Kubo-Greenwood formula shows that conduction may be expected if there are degenerate states at the Fermi level, following Mott and Davis [35]). We study the doping dynamics based on the concept of correlating this ξ with other dynamical variables such as fluctuations in structure or H hopping. As we indicate in the Introduction, thermal motion and H hopping can have a significant role in modulating the electronic eigenvalues near the Fermi level. We also study the change in coordination number of the hydrogen and its correlation with ξ. Of course, the study of ξ and its time evolution does not completely treat the doping problem. Conduction is possible only if states are extended in the sense of Anderson [36], Dong [37], and Drabold [38]. Still, as we argue below from the Kubo-Greenwood formula, the condition for charge transport in the presence of (extended) occupied and unoccupied states nearly degenerate with the Fermi level.

This study can be related to the noise power fluctuation experiment by Parmen, which shows that resistance in doped a-Si:H is sensitive to a small number of fluctuations and changes with time. It is observed that the motion of the bonded hydrogen is correlated with variations in the resistance [39]. We present here the dynamics of the doped a-Si:H and observe the fluctuation in the conductivity due to the motion on the hydrogen in the network.

A. Energy gap and Kubo-Greenwood formula

To develop this picture a bit further, we remind the reader that the conductivity for disordered solid can be expressed from microscopic quantities (wave functions, eigenvalues, etc.) with the Kubo-Greenwood formula [40,41]. For a very clear derivation and elementary applications, see Mott and Davis [35]. As it is usually interpreted, this result is applied to a static configuration of a lattice. We extend this idea elsewhere by adopting an adiabatic picture in which we thermally average the Kubo-Greenwood formula over a long constant temperature MD simulation to pick up thermal effects on carrier transport (for details, see Ref. [42]). In practice, this amounts to computing:

$$\sigma_{\mathrm{dc}} = \frac{2\pi e^2 \hbar \Omega}{m^2} \overline{|D_{\epsilon_F}|^2 N^2(\epsilon_F)}. \qquad (1)$$

Here, the bar indicates thermal or trajectory average, D_{ϵ_F} is a matrix element of $\partial/\partial x$ between single-particle (Kohn-Sham) states near the Fermi level, Ω is the cell volume, and $N(\epsilon_F)$ is the density of states. This expression emphasizes that dc conduction may occur when (i) the density of states at the Fermi level is nonzero, and (ii) the momentum matrix element is also nonvanishing. It implies that conduction accrues for instantaneous configurations that support the conditions (i) and (ii).

In Fig. 12, we reveal the fluctuations in energy eigenvalues for the highest three valence-band and lowest three conduction-band states. The upper panel of Fig. 12(a) is for B-doped a-Si without hydrogen, and the lower panel is B-doped a-Si with hydrogen. In B-doped a-Si, the HOMO LUMO gap is small enough to consider the system to be conducting. Upon addition of H, there is thermal modulation of both the HOMO and LUMO states, which can be seen in the lower panel of Fig. 12(a). At a certain interval in the thermal simulation, the HOMO LUMO levels overlap, and it is the highly conducting configuration according to KGF. The period for which the HOMO LUMO gap (ξ) opens up is the nondoping configuration.

In P-doped a-Si, the HOMO level is shifted towards the LUMO level, and the HOMO LUMO gap is almost zero for most of the simulation time, which can be seen in Fig. 12(b). There is a small fluctuation in the HOMO level around 20 to 30 ps that changes the system to the nondoping mode, which is due to the change in the structure of P from fourfold to threefold and twofold. We can say that threefold and twofold P are undoped

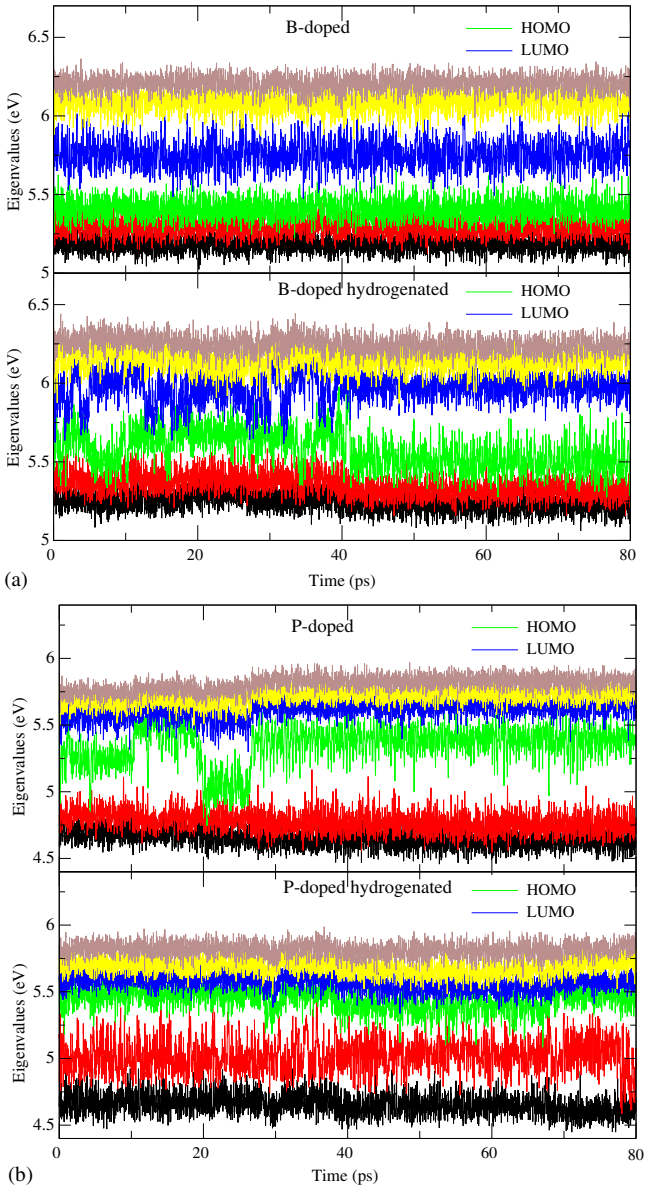

FIG. 12. Plot of the highest three valence-band and the lowest three conduction-band energy levels. (a) For B-doped and hydrogenated B-doped a-Si at 600 K. (b) For P-doped and hydrogenated a-Si at 600 K. HOMO level (green); LUMO level (blue). Proximity of the green and blue levels implies conduction is possible (the HOMO LUMO gap is small).

configurations. When H is added to the P-doped a-Si, the system becomes n-type doped with the HOMO and LUMO levels overlapped. This again demonstrates the n-type behavior of H in the network. The network rearranges to give the tetrahedral P [Fig. 12(b)].

B. Hydrogen hopping and coordination number

We add the n-type (P) and p-type (B) impurities in the network of a-Si by substitutional method and then carry out thermal simulation. Hydrogen atoms are added to

determine the effect of H on the dynamics of doping and conduction. The H atom is placed at various Si—Si bond centers at varying distances from the impurities atoms in doped *n*-type (P-doped) and *p*-type (B-doped) *a*-Si models.

The variation of the distance of hydrogen from the impurities for different temperatures is shown in Fig. 13. The main purpose of this calculation is to determine a range (distance from B) for which the H is attracted. Our calculations show that the hydrogen in a network is attracted towards the impurity sites, doubtless to reduce strain in the region containing the dopant. In both the B- and P-doped hydrogenated systems, hydrogen tends to move towards the impurities. The motion is significant only at sufficiently high temperature. For 300 K, in B-doped hydrogenated *a*-Si, it is seen that the motion of hydrogen is almost insignificant on the time scale of our simulation. The prominent movement towards the impurity is visible for P-doped hydrogenated *a*-Si [Fig. 13(b)], where it can be clearly seen that for 600 and 800 K the thermal energy is sufficient for H to move towards the P atoms. At 1000 K, the H atom sticks to the B (not shown here), which helps us conclude that if the thermal energy is sufficient, then H atoms eventually move toward the impurity sites.

We perform a microscopic study on the motion of hydrogen in the system and the change in its coordination number. We find that H in the network is mobile, and its hopping changes the structure and dynamics of the network. By tracking the motion of the hydrogen atoms, we observe that the H atom prefers to move towards the B or P sites by hopping through various bond sites, providing strong evidence that H atoms in an *a*-Si network are highly mobile and have higher affinity for the impurities. Another important feature that we notice in the study of hydrogen hopping is the significant decrease in the HOMO LUMO gap (ξ) in the region where H-atom coordination changes rapidly from free to singly coordinated and then to twofold as shown in Fig. 14. The coordination cutoff distance for the H—Si bond is taken as 1.65 Å for calculations.

In an undoped *a*-Si network, H prefers to stay in the sites of highly distorted bonds and bond angles. When B and P are introduced in a perfectly tetrahedral site in an *a*-Si network, they introduce strain (especially B). So, the region becomes distorted, and the H atoms introduced in such network tend to move towards those regions. From a different perspective, as H bonds more strongly with B than with Si (bond dissociation energy of B—H is 3.52 eV and Si—H is 3.10 eV) [43], in B-doped *a*-Si, H moves towards B due to the strain and also prefers to bond with B rather than Si. This is consistent with NMR experiments which predict that about 40% of H atoms in P-doped *a*-Si:H are in the first nearest neighbor of B [9]. In contrast, H bonds similarly with P and Si (the bond dissociation energy of P—H is 3.08 eV and Si—H is 3.10 eV) [43] and seems consistent with the result of NMR that about 40% of H atoms in P-doped *a*-Si:H are in the second-nearest-neighbor shell of P [9].

Doping phenomena are influenced by the motion of hydrogen in the network. Figure 14 shows the hopping of the H atom from various bond centers to passivating the dangling bond at 12.78, 24, 59.146, and 79.64 ps snapshots for B-doped hydrogenated *a*-Si at 600 K. This is consistent with the noise power fluctuations experiment by Kakalios and co-workers, which suggests that the rearrangement of hydrogen-bonding configurations that involves the collective motion of many hydrogen atoms changes the electronic properties of *a*-Si:H [39].

A goal of this paper is to bring forth a new suggestion that the motion of H and its changing coordination in the network affects the doping significantly. This feature can be

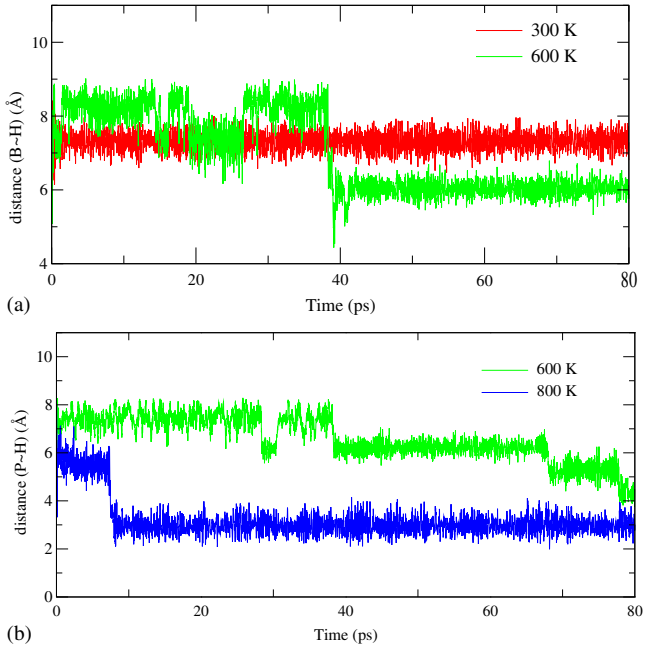

FIG. 13. Distance between hydrogen and impurities. (a) B-doped hydrogenated *a*-Si. (b) P-doped hydrogenated *a*-Si (red, 300 K; green, 600 K; blue, 800 K).

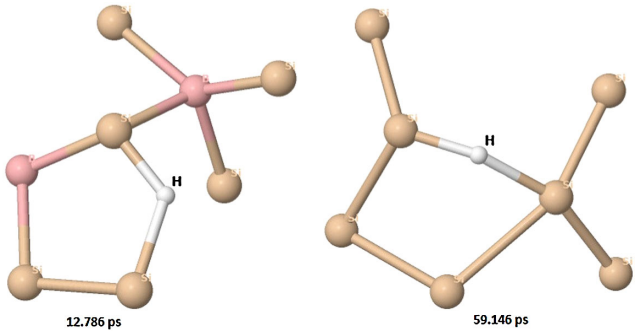

FIG. 14. Hydrogen hopping between bond centers and passivating the Si dangling bonds in hydrogenated B-doped *a*-Si DB at various snapshots for 600 K thermal MD.

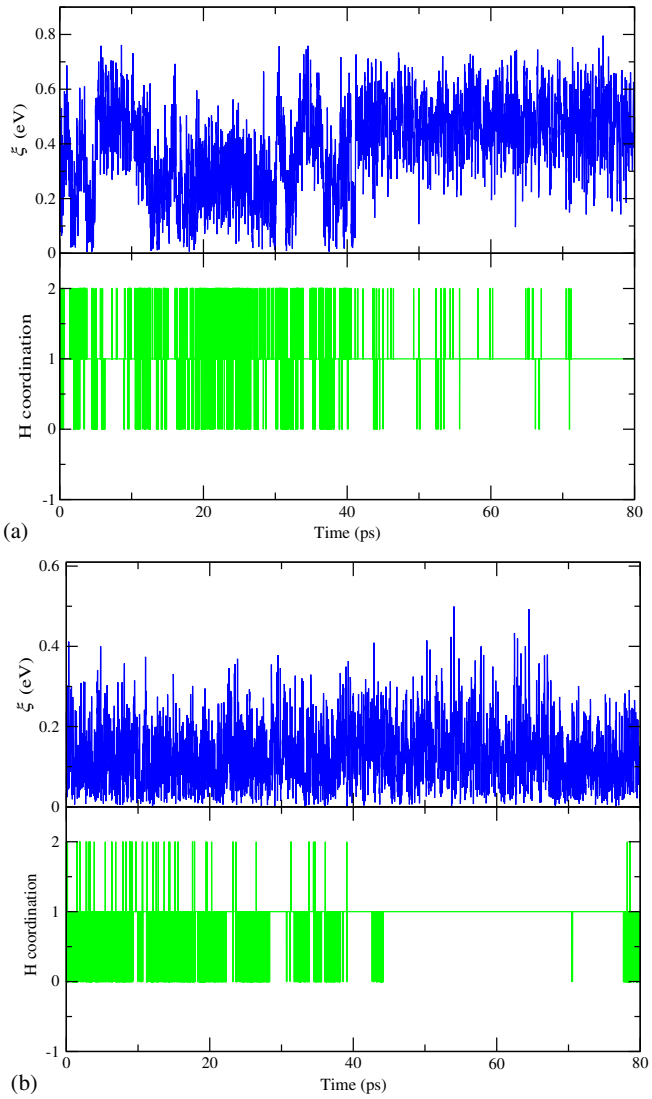

FIG. 15. (Lower half) Hydrogen coordination fluctuation. (Upper half) Energy-gap fluctuation. (a) B-doped hydrogenated *a*-Si. (b) P-doped hydrogenated *a*-Si. Zero coordination means H is in process of hopping.

seen clearly in Fig. 15(a) for B-doped hydrogenated *a*-Si at 600 K between 10 and 40 ps time where the energy gap decreases significantly. In hydrogenated P-doped *a*-Si [Fig. 15(b)], although the coordination of the H atom fluctuates in the beginning, at later times it forms a single bond with Si, thereby passivating the DB, which is as expected from the doping point of view, because in *n*-type doping, both P and H assist doping, and the energy gap is small. The B atoms substituted in tetrahedral Si atom sites have consistent fourfold coordination, while the coordination of P changes from four- to threefold and sometimes even twofold. We find that this change in the coordination of P atoms has a significant effect in the doping process as the study of dynamics with P atoms not substituted in the perfectly tetrahedral Si sites will result in an undoped system, which is quite consistent with the experimental results.

V. CONCLUSION

Our calculations suggest that although Mott's view is correct that nontetrahedral impurities do not dope an *a*-Si network, this is only part of the story of low doping efficiency. H passivation and the special attraction of H to impurities is also a key to understanding low doping efficiency. B substituted into a tetrahedral Si site creates a substantial strain in local bonding, which attracts H atoms and induces H passivation and doping suppression. In P-doped *a*-Si, bonds are less strained compared to B-doped *a*-Si and H passivation follows similarly.

It is shown in the work of Abtew and co-workers [5,8] that H is highly mobile. This mobility can lead to fluctuations in the HOMO LUMO gap (denoted by ξ in this paper) that also strongly affect conductivity.

ACKNOWLEDGMENTS

We thank the Army Research Office for supporting this work, as well as the Ohio Supercomputer Center for an allocation of computer time.

[1] B. Fieque, J. L. Tissot, C. Trouilleau, A. Crastes, and O. Legras, Uncooled microbolometer detector: Recent developments at Ulis, Infrared Phys. Technol. **49**, 187 (2007).
[2] R. A. Street, *Hydrogenated Amorphous Silicon* (Cambridge University Press, Cambridge, England, 1991).
[3] W. E. Spear and P. G. LeComber, Substitutional doping of amorphous silicon, Solid State Commun. **17**, 1193 (1975).
[4] J. Ziman, *Models of Disorder: The Theoretical Physics of Homogeneously Disordered Systems* (Cambridge University Press, Cambridge, England, 1979).
[5] D. A. Drabold, T. A. Abtew, F. Inam, and Y. Pan, Network structure and dynamics of hydrogenated amorphous silicon, J. Non-Cryst. Solids **354**, 2149 (2008).
[6] P. A. Fedders and D. A. Drabold, Molecular dynamics investigation of conformational fluctuations and low energy vibrational excitations in *a*-Si:H, Phys. Rev. B **53**, 3841 (1996).
[7] R. Atta-Fynn, P. Biswas, and D. A. Drabold, The electron-phonon coupling is large for localized states, Phys. Rev. B **69**, 245204 (2004).
[8] T. A. Abtew, F. Inam, and D. A. Drabold, Thermally stimulated H diffusion and emission in hydrogenated amorphous silicon, Europhys. Lett. **79**, 36001 (2007).
[9] J. B. Boyce and S. E. Ready, Nuclear-magnetic-double-resonance investigation of the dopant microstructure in hydrogenated amorphous silicon, Phys. Rev. B **38**, 11008 (1988).
[10] P. A. Fedders and D. A. Drabold, Theory of boron doping in *a*-Si:H, Phys. Rev. B **56**, 1864 (1997).

[11] B. Cai and D. A. Drabold, Theoretical studies of structure and doping of hydrogenated amorphous silicon, Mater. Res. Soc. Symp. Proc. **1321** (2011).

[12] J. Liang, E. A. Schiff, S. Guha, B. Yan, and J. Yang, Hole-mobility limit of amorphous silicon solar cells, Appl. Phys. Lett. **88**, 063512 (2006).

[13] M. Cliffe, M. T. Dove, D. A. Drabold, and A. L. Goodwin, Structure determination of disordered materials from diffraction data, Phys. Rev. Lett. **104**, 125501 (2010).

[14] D. A. Drabold, Y. Li, B. Cai, and M. Zhang, Urbach tails of amorphous silicon, Phys. Rev. B **83**, 045201 (2011).

[15] Y. Pan, F. Inam, M. Zhang, and D. A. Drabold, Atomistic origin of Urbach tails in amorphous silicon, Phys. Rev. Lett. **100**, 206403 (2008); Y. Pan, M. Zhang, and D. A. Drabold, Topological and topological-electronic correlations in amorphous silicon, J. Non-Cryst. Solids **354**, 3480 (2008).

[16] J. Heyd, G. E. Scuseria, and M. Ernzerhof, Hybrid functionals based on a screened Coulomb potential, J. Chem. Phys. **118**, 8207 (2003).

[17] G. Kresse and J. Furthmuller, Efficient iterative schemes for ab initio total-energy calculations using a plane-wave basis set, Phys. Rev. B **54**, 11169 (1996).

[18] G. Kresse and J. Joubert, From ultrasoft pseudopotentials to the projector augmented-wave method, Phys. Rev. B **59**, 1758 (1999).

[19] G. T. Barkema and N. Mousseau, High-quality continuous random networks, Phys. Rev. B **62**, 4985 (2000).

[20] F. Wooten, K. Winer, and D. Weaire, Computer generation of structural models of amorphous Si and Ge, Phys. Rev. Lett. **54**, 1392 (1985).

[21] D. B. Saint John, H.-B. Shin, M.-Y. Lee, S. K. Ajmera, A. J. Syllaios, E. C. Dickey, T. N. Jackson, and N. J. Podraza, Influence of microstructure and composition on hydrogenated silicon thin film properties for uncooled microbolometer applications, J. Appl. Phys. **110**, 033714 (2011).

[22] I. Santos, P. Castrillo, W. Windl, D. A. Drabold, L. Pelaz, and L. A. Marques, Self-trapping in B-doped amorphous Si: Intrinsic origin of low acceptor efficiency, Phys. Rev. B **81**, 033203 (2010).

[23] H.-B. Shin, D. B. Saint John, M.-Y. Lee, N. J. Podraza, and T. N. Jackson, Electrical properties of plasma enhanced chemical vapor deposition a-Si:H and a-$Si_{1-x}C_x$:H for microbolometer applications, J. Appl. Phys. **114**, 183705 (2013).

[24] A. Heredia, A. Torres, A. Jaramillo, F. J. De la Hidalga, and A. Munguia, Properties of boron doped amorphous silicon films obtained with a low frequency plasma, in *Proceedings of the 14th International Symposium on Plasma Processing, 2002* (unpublished), pp. 10–16.

[25] P. Alpuim, V. Chu, and J. P. Conde, Electronic and structural properties of doped amorphous and nanocrystalline silicon deposited at low substrate temperatures by radio-frequency plasma-enhanced chemical vapor deposition, J. Vac. Sci. Technol. A **21**, 1048 (2003).

[26] D. B. Saint John, H.-B. Shin, M.-Y. Lee, E. C. Dickey, N. J. Podraza, and T. N. Jackson, Thin film silicon and germanium for uncooled microbolometer applications, Proc. SPIE Inf. Technol. Appl. **8012**, 80123U (2011).

[27] R. W. Collins, A. S. Ferlauto, G. M. Ferreira, C. Chen, J. Koh, R. J. Koval, Y. Lee, J. M. Pearce, and C. R. Wronski, Evolution of microstructure and phase in amorphous, protocrystalline, and microcrystalline silicon studied by real time spectroscopic ellipsometry, Sol. Energy Mater. Sol. Cells **78**, 143 (2003).

[28] A. H. M. Smets, W. M. M. Kessels, and M. C. M. van de Sanden, Vacancies and voids in hydrogenated amorphous silicon, Appl. Phys. Lett. **82**, 1547 (2003).

[29] A. H. M. Smets and M. C. M. van de Sanden, Relation of the Si—H stretching frequency to the nanostructural Si—H bulk environment, Phys. Rev. B **76**, 073202 (2007).

[30] J. Melskens, A. H. M. Smets, M. Schouten, S. W. H. Eijt, H. Schut, and M. Zeman, New insights in the nanostructure and defect states of hydrogenated amorphous silicon obtained by annealing, IEEE J. Photovoltaics **3**, 65 (2013).

[31] D. B. Saint John, H. Shen, H.-B. Shin, T. N. Jackson, and N. J. Podraza, Infrared dielectric functions of hydrogenated amorphous silicon thin films determined by spectroscopy ellipsometry, in *Proceedings of the 38th Photovoltaic Specialists Conference, 2012*, p. 003112, http://ieeexplore.ieee.org/xpls/abs_all.jsp?arnumber=6318239.

[32] N. J. Podraza, J. Li, C. R. Wronski, M. W. Horn, E. C. Dickey, and R. W. Collins, Analysis of compositionally and structurally graded Si:H and Si1-xGex:H thin films by real time spectroscopic ellipsometry, Mater. Res. Soc. Symp. Proc. **1066**, 1066-A10-01 (2008).

[33] S. C. Shen and M. Cardona, Infrared and far infrared absorption of B- and P-doped amorphous Si, J. Phys. (Paris), Colloq. **42**, C4-349 (1981).

[34] N. Ross, K. Shrestha, O. Chyan, C. L. Littler, V. C. Lopes, and A. J. Syllaios, Characterization of boron doped amorphous silicon films by multiple internal reflection infrared spectroscopy, Mater. Res. Soc. Symp. Proc. **1536**, 127 (2013).

[35] N. F. Mott and E. A. Davis, *Electronic Processes in Non-Crystalline Materials* (Clarendon, Oxford, 1991).

[36] P. W. Anderson, Absence of diffusion in certain random lattices, Phys. Rev. **109**, 1492 (1958).

[37] J. Dong and D. A. Drabold, Band-tail states and the localized-to-extended transition in amorphous diamond, Phys. Rev. B **54**, 10284 (1996).

[38] D. A. Drabold, Topics in the theory of amorphous materials, Eur. Phys. J. B **68**, 1 (2009).

[39] C. E. Parman, N. E. Israeloff, and J. Kakalios, Conductance-noise power fluctuations in hydrogenated amorphous silicon, Phys. Rev. Lett. **69**, 1097 (1992).

[40] R. Kubo, Statistical-mechanical theory of irreversible processes. I. General theory and simple applications to magnetic and conduction problems, J. Phys. Soc. Jpn. **12**, 570 (1957).

[41] D. A. Greenwood, The Boltzmann equation in the theory of electrical conduction in metals, Proc. Phys. Soc. London **71**, 585 (1958).

[42] T. A. Abtew, M. Zhang, and D. A. Drabold, Phys. Rev. B **76**, 045212 (2007).

[43] *CRC Handbook of Chemistry and Physics*, edited by D. R. Lide (CRC Press, Boca Raton, 2005).